To be published in Optics Letters:

Title: Composite material anti-resonant optical fiber electromodulator with 3.5 dB depth

Authors: Adam Lewis,Francesco De Lucia,Walter Belardi,Chung Che Huang,John Hayes,Francesco Poletti,Daniel William Hewak,Pier Sazio

Accepted: 15 December 19

Posted 16 December 19

DOI: https://doi.org/10.1364/OL.382921

Composite material anti-resonant optical fiber electromodulator with 3.5 dB depth

ADAM H. LEWIS[1], FRANCESCO DE LUCIA[1], WALTER BELARDI[2], CHUNG-CHE HUANG[1], JOHN R. HAYES[1], FRANCESCO POLETTI[1], DAN HEWAK[1], AND PIER J.A. SAZIO[1*]

[1]*Optoelectronics Research Centre, University of Southampton, Highfield, Southampton, Hampshire. SO17 1BJ, UK*
[2]*Université de Lille, CNRS, UMR 8523 –PhLAM – Physique des Lasers Atomes et Molécules, F-59000 Lille, France*

**Corresponding author: P.A.Sazio@soton.ac.uk*

Received XX Month XXXX; revised XX Month, XXXX; accepted XX Month XXXX; posted XX Month XXXX (Doc. ID XXXXX); published XX Month XXXX

The hollow regions of an anti-resonant fiber (ARF) offer an excellent template for the deposition of functional materials. When the optical properties of such materials can be modified via external stimuli, it offers a method to control the transmission properties of the fiber device. In this letter, we show that integration of a MoS_2 film into the ARF voids allows the fiber to act as an electro-optical modulator. We record a maximum modulation depth of 3.5 dB at 744 nm, with an average insertion loss of 7.5 dB.

http://dx.doi.org/10.1364/OL.99.099999

Alternatives to step index fibers such as hollow core optical fiber geometries are becoming increasingly relevant to modern telecommunications systems, with recent results showing low loss on kilometer scales [1]. One such structure is the anti-resonant fiber (ARF) that is able to guide light in the air core using a variety of cladding architectures. Intriguingly, the high internal surface area presented by this waveguide geometry offers an ideal materials deposition template for strong light-matter interaction. We have previously demonstrated [1] that 300 nm thick silicon layers deposited conformally within an 8-ring tubular borosilicate cladding creates a novel composite material ARF (CM-ARF). The waveguide properties are theoretically identical to that of a single material ARF with an equivalent refractive index and core wall thickness. This suggests that only the optical path travelled by light at the core boundary is relevant for antiresonance guidance, thus opening the possibility of exploiting the active properties of materials selectively added to the basic air-silica design. This could include for example, the free carrier plasma dispersion effect, in which the change of refractive index and absorption resulting from a change in the concentration of free carriers (either photo- or electric field induced) could be used to achieve intensity or phase modulation [2]. CM-ARF designs therefore allow the otherwise passive photon transport properties of standard ARF air-silica waveguides to be actively managed and controlled. However, in order to minimize waveguide losses due to addition of functional materials at the core boundary, it is necessary to reduce layer thicknesses by an order of magnitude, as even the deposition of 300 nm of silicon substantially alters transmission properties [1].

Motivated by this requirement and for a more benign semiconductor deposition technology that does not require the use of toxic and highly pyrophoric precursors such as silane gas [1], we investigated the growth of 2D Transition Metal Dichalcogenide (2D TMDC) layers inside the fibers. These semiconductors are typically sub-10 nm in thickness, making them ideal materials for creating CM-ARF active devices exhibiting relatively low optical losses. Furthermore, the ability of TMDC materials to grow on amorphous substrates under benign, low temperature conditions was a major consideration in our synthesis protocol.

We note that there already exist numerous examples of 2D TMDCs being used with conventional solid core optical fibers and planar devices [3,4]. Typically, the combination of these monolayers with incumbent fiber technologies exploits the imaginary component of the third order nonlinear susceptibility to create saturable absorbers in mode-locked and Q-switching lasers. However, in order to avoid the high peak powers required to induce such modulation in 2D materials, our aim is to produce optical control at power levels more compatible with datacom. To this end, we note that electrostatic gate tunable electro-absorption has recently been observed in silicon backgated TMDC planar (normal incidence, non-waveguide) device geometries. Evidence of such are reported by Yu et al. [5], or ITO backgated Hafnia/MoS_2 structures fabricated by Vella et al. [6]. In this Letter, we offer an alternative method of electro-optic modulation through the use of a functionalized hollow core fiber waveguide. As shown in Fig. 1, the ARF used as the deposition template was fabricated in-house at the ORC in Southampton. It has a 50 μm core diameter and a

surrounding ~20 μm triangular cladding region with 800 nm silica strut thicknesses. The optical transmission characteristics of the pristine (i.e. non functionalized) ARF are shown in Fig. 1(b) as determined by launching blackbody radiation from a white light source into the waveguide. For the subsequent 2D materials functionalization, we considered a number of deposition techniques. For high quality wafer-scale growth, bottom-up methods such as Chemical Vapour Deposition (CVD) and Atomic Layer Deposition (ALD) are frequently employed. However, leaving aside the difficulty of replicating these (typically low pressure) growth parameters within the highly confined ARF internal structure, TMDC chemical vapour deposition processes demand high temperature (~1000 °C) annealing to create high quality 2D material. This can embrittle and strongly compromise the structural integrity of the ARF template. In order to circumvent these practical issues, we followed instead a solution-based thermal decomposition processing method first discussed by Liu et al. [7] who used a mixture of dimethylformamide (DMF) with an ammonium tetrathiomolybdate, $(NH_4)_2MoS_4$ single source precursor. Yang et al. [8] further improved the wettability of the solvent through the introduction of aminoethanol and butylamine to the solvent solution. Following this work, we prepared a solution of 0.1 g of single source precursor dissolved in a mixture of 4.5 ml butylamine, 4.5 ml dimethylformamide and 1 ml of aminoethanol. This solution was infiltrated into the ARF hollow regions shown in Fig. 1(a) by capillarity, until approximately 0.3 m of the 0.8 m long fiber had

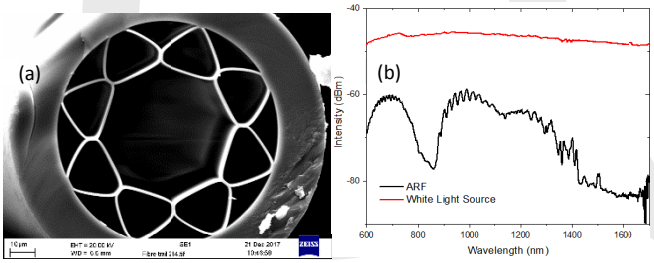

Fig. 1. The ARF template used in this letter. (a) A SEM image of the fiber. The core diameter is 50 μm, with the cladding struts of 800 nm thickness. (b) The optical transmission spectra of the pristine ARF in comparison to characteristics of the white light source input.

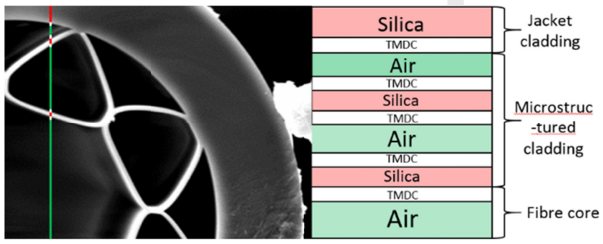

Fig. 2. Cross-section through the ARF template as indicated by multicolored line from the air-core center to outer glass cladding jacket. The color coded layer schematic of functionalized Composite Material ARF is described by the multicolored line. Alternating, repeating layers and boundaries of air, silica and TMDC (not to scale) are present and labelled according to their location within the ARF.

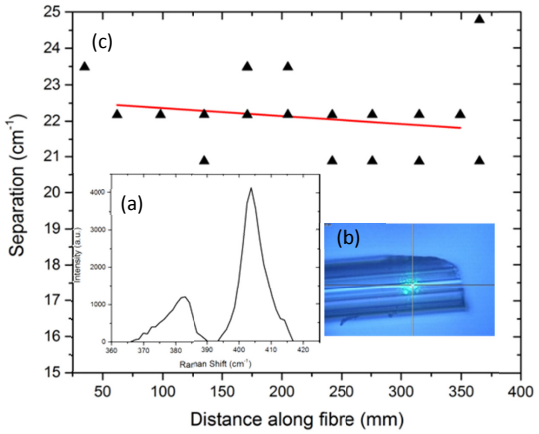

Fig. 3. (a) A typical spectrum from the MoS_2 CM-ARF showing the E^1_{2g} and A_{1g} Raman modes. (b) The laser is focused through the silica host material and onto the deposited MoS_2. This produces a large silica background, which has been removed from the data in (a) and Raman analysis in (c). The least squares fit of (c) with the central 30 cm of deposition shows a 22cm^{-1} peak separation indicative of bilayer thickness.

been filled. This was followed by annealing in air for 10 min at 90 °C. The fiber was placed into a furnace and heated at 26 mbar pressure with 100 sccm of 6% H_2/Ar flow for 2 hours at 500 °C. This resulted in the composition seen in Fig. 2, a cross-sectional view of how the deposition occurs in hollow regions of the fiber.

To characterize the synthesized MoS_2, the CM-ARF was analyzed using a Renishaw InVia micro-Raman system. All measurements were performed using 532 nm excitation wavelength, with 20 mW incident power and 50x (0.63 NA) objective. This allows for a non-destructive probe to determine both the film quality and thickness. A typical Raman response obtained from our CM-ARF in Fig. 3(a), shows the in-plane E^1_{2g} and the out-of-plane A_{1g} Raman modes, located at 382.9 cm^{-1} and 403.8 cm^{-1}, respectively. For TMDC films, it is well known [9] that the wavenumber separation of the Raman peaks is strongly indicative of the number of layers present. Fig. 3(a) shows a separation of 20.9 cm^{-1}, corresponding to a bilayer film thickness. However, the 7.2 cm^{-1} Full Width at Half Maximum (FWHM) of the peaks suggests a polycrystalline deposition. The fiber was analyzed with the 532 nm excitation laser focused through the silica cladding as seen in Fig. 3(b). A baseline measurement of the data was therefore also performed to remove the silica Raman background and any additional scattering noise.

In order to analyse the uniformity of the MoS_2 film that was selectively deposited longitudinally within the 80 cm long CM-ARF, Raman spectra were obtained at numerous locations spaced along the fiber as shown in Fig. 3(c). This graph exhibits a clear trend, with a least squares fit of the central 30 cm region of the deposition showing a 22cm^{-1} peak separation indicative of bilayer thickness within the limits of measurement error. However, it can be seen that the beginning and end regions of the deposition exhibit a more bulk-like MoS_2 Raman response. This is due to limitations of the furnace used to anneal the fiber – the entrances of the furnace are more likely to be non-uniform in heat distribution. Thus, this facile deposition process can potentially fill fiber lengths on meter scales with high uniformity, limited only by furnace length and geometry. In addition, as well as longitudinal control over the 2D TMDC deposition process, we can further manipulate the properties of our CM-ARF via selective axial deposition within the

hollow template structure. As can be seen from the spectra in Fig. 4, well established [10] selective filling techniques for microstructured optical fibers can be readily deployed to deposit within the central core region only, the cladding region only, or simply coating the entire internal structure (as in Fig. 2). Here, in order to further highlight the materials versatility of our technique, the CM-ARF of Fig. 4 was created using an ammonium tetrathiotungstate $(NH_4)_2WS_4$ single source precursor followed by a similar thermal processing protocol to the $(NH_4)_2MoS_4$ solutions detailed earlier. Raman analysis of the subsequently deposited WS_2 layers exhibited in-plane E^1_{2g} /2LA(M) resonant phonon modes [11] and the out-of-plane A_{1g} Raman mode, located at ~351 cm^{-1} and ~413 cm^{-1}, respectively. The intensity of the peaks shows a 1:1 ratio common for bilayer deposition when excited with a 532 nm laser. Similarly to MoS_2, the 9.9 cm^{-1} FWHM of the Raman peaks in Fig. 4 inset indicated a polycrystalline deposition of 30 cm within the total 80 cm fiber length.

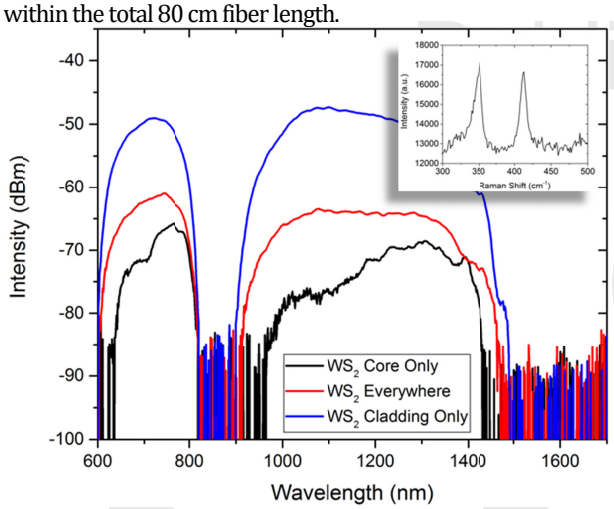

Fig. 4. White light optical transmission properties of WS_2 CM-ARF waveguides with identical initial template structures (as shown in Fig. 1) but functionalized with three different axially selective depositions. The inset shows a typical Raman image of the deposited WS_2 film.

The optical transmission properties of the CM-ARF axially selective depositions shown in Fig. 4 were measured using a Bentham WLS100 white light source connected to a conventional step-index multimode fiber. This was then butt-coupled to the CM-ARF, which in turn was connected to an Optical Spectrum Analyser (OSA) (Yokogawa AQ6370) using bare fiber adaptors. The fiber was kept as straight as possible to mitigate bend loss. Due to the relatively short 80 cm length of the fiber, multimodal interference occurs and is visible in the spectra. This can be observed especially in the fluctuating peaks of the 600 – 800 nm anti-resonant window of the pristine ARF in Fig 1(b). The CM-ARF transmission spectrum shows the greatest change when the WS_2 is deposited in the core region only. This is likely due to a higher modal interaction with the 2D material. Somewhat counterintuitively, given the presence of additional material, the spectrum in which WS_2 is deposited in both the core and cladding regions of the fiber shows comparably lower losses, suggesting that the anti-resonant properties may have been modified, thus allowing the mode to experience greater confinement. This appears to be confirmed by the cladding only deposition, which also enhances the mode confinement and exhibits the lowest optical loss, i.e. the lowest light-matter interaction of all three configurations. Therefore, for optimised 2D layer interaction with modest scattering loss, the CM-ARF configuration with materials deposited in all regions of the fiber (i.e. identical to the MoS_2 configuration shown in Fig. 2) was ideal for further investigation in electro-optic experiments.

Comparison of the white light optical transmission characteristics of a 90 cm long pristine ARF shown in Fig. 1, with the 80 cm long MoS_2 CM-ARF of Fig. 5a results in an average insertion loss due to the TMDC layers of around 7.5 dB in the 603 nm to 775 nm anti-resonant region. The short length of the empty ARF control sample means that its overall optical loss is very low, resulting in relatively shallow resonant dips in the spectrum compared with the lossier MoS_2 CM-ARF. Electro-optical control measurements were also performed on the empty ARF. The fiber was placed on a 30 cm long metallic strip to which a voltage of 1500 V was applied (maximum available with our setup without inducing an undesirable arc discharge) whilst simultaneously analyzing the white light spectrum with the OSA. As expected, the externally applied electric field did not alter the transmission characteristics in any way. In contrast, when the same experiment was repeated using the MoS_2 CM-ARF with the functionalized length fully located onto the electrode, the entire output spectrum decreased in intensity, exhibiting a maximum modulation depth of 3.52 dB at 744.2 nm, as shown in Fig. 5(b). Lower applied voltages also resulted in the spectrum being modified, albeit with smaller modulation depths. Identical experiments with the WS_2 CM-ARF also resulted in the observation of electro-optic modulation as we previously reported in [12], but with a weaker effect (1.4 dB maximum modulation depth at 740 nm with 1000 V applied). This difference in performance is likely due to some subtle complexities associated with the two slightly different deposition chemistries; compared with the tetrathiomolybdate single source precursor, ammonium tetrathiotungstate is somewhat more challenging to work with due to low co-ordination with common solvents. This tends to inhibit the formation of uniform, continuous precursor films on glass or crystalline substrates [13].

As shown in Fig. 5, although the electro-modulation depth of these devices is at its maximum at around 744 nm, implying some component of excitonic absorption, the overall electro-absorption effect was observed over a very broad spectral range. This strongly suggests that plasma dispersion is the dominant mechanism, which typically operates over broad wavelength regimes due to the presence of free charge carriers [2,6]. The CM-ARFs can therefore be considered as prototype "Optical Field Effect Transistor (FET) waveguides", in which the capacitively coupled, insulated external gate (as presented by the metallic strip and optical fiber silica cladding) induces electrostatic doping of the 2D layer semiconductor Fermi levels. This results in the modulation of propagating optical signals. A complete analysis of the total electric field experienced by all the MoS_2 layers shown in Fig. 2, and thus the expected change in carrier density due to the field effect and corresponding shift in Fermi energy, is convoluted due to the presence of so many different dielectric layers and regions. Nevertheless, a simple estimate can be made of the magnitude of electric field present at the very first silica/MoS_2 interface, following the multicolored solid line in Fig. 2 from the outside of the fiber towards the central air core. Given an externally applied voltage of 1500 V, an outer silica jacket cladding thickness of 15 µm, (and dielectric constant, 3.8) the transverse electric field in the first MoS_2 layer is approximately 2.6 x 10^7 V/m. Following the analysis of Vella et al. [6], a plane of electrostatically induced

surface charge density σ that is required to generate an exactly opposing electric field which will fully screen the externally applied field, is given by the equation $E = \sigma e/(2\varepsilon_r\varepsilon_0)$, which for MoS_2 ($\varepsilon_r = 7$) requires $\sigma = 2 \times 10^{12}$ electrons/cm^2, where e is the charge of an electron, ε_0 is the permittivity of free space and ε_r is the relative permittivity of MoS_2. This change in carrier density translates to a shift of the Fermi energy [14] (given by $(\pi(h/2\pi)^2 n)/m_e$ where n is the carrier concentration, h is Planck's constant and $m_e \sim 0.3m_0$ is the effective electron mass in the MoS_2 layer) of approximately 16 meV.

Although any additional electro-absorption due to this increase in carrier concentration in a 2D layer located on the outer periphery of the CM-ARF shown in Fig. 2 is likely to be relatively small, the experimentally observed large overall enhancement of 3.52 dB shown in Fig. 5 may be an inherent property of our anti-resonant waveguide design. We hypothesize that this is due to the current interpretation of optical guidance through anti-resonance [15] in which the core wall interface can be considered as a resonant Fabry-Perot cavity. Wavelengths not in resonance are reflected back into the core and thus propagate with low loss. Therefore active properties of functional materials selectively added here will be strongly enhanced thanks to this transverse Fabry-Perot multi-pass geometry in combination with a highly extended fiber waveguide for very efficient light-matter interaction.

Typical modulator performance figures of merit for datacom applications are of the order of 7 dB modulation depth and <2 dB insertion loss [6]. Although our prototype CM-ARF electro-absorption modulators do not yet match these criteria with 3.52 dB depth and 7.5 dB loss, our unique CM-ARF Optical FETs operate over a very wide spectral range, creating many opportunities for implementation as well as potential performance enhancements. The voltage requirements are a primary target for next generation prototypes. As seen from the analysis above, kV level potential differences applied externally to the fiber are required to create sufficient carrier concentrations for adequate modulation depths to be observed. This can be substantially improved by redesigning both the outer silica jacket cladding and the antiresonant internal structure. In this case, a more conventional and simpler tubular ARF design such as one we have used previously [1] will minimize the number of dielectric layers and regions to reduce the internal electric fields. This can then be combined with voids in the outer silica cladding that can be filled with liquid metals such as gallium [16] to create internal electrodes. Lower operating voltages are also highly beneficial in terms of reduced $CV^2/2$ switching energies and RC time constants for optimizing f_{max} clock rates in datacom relevant system devices. These can then be fully fiberized, potentially allowing for seamless integration with incumbent telecoms infrastructure, avoiding the need to interface and couple with conventional planar electro-optic modulator technologies.

In conclusion, we have created a novel, active CM-ARF technology platform with excellent potential for all-fiber electro-optics. Selective deposition of functional materials highlights the outstanding versatility of our technique. This could allow for the creation of structural complexity such as form birefringence with electro-optically tunable polarisation control for example. Further augmented via the addition of different 2D layers, alloys, heterostructures and other exotica such as Weyl or Dirac topological semimetals (e.g. WTe_2, $MoTe_2$) with unconventional E-k dispersion properties [17] could lead to very strongly enhanced Fermi level tuning with applied electric fields.

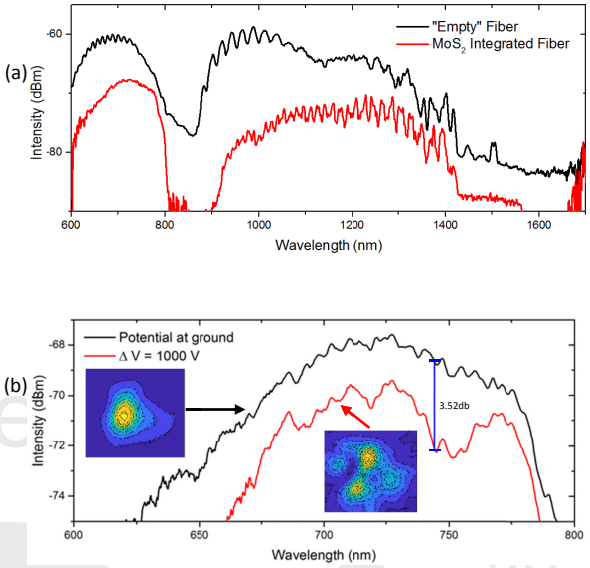

Fig. 5. (a) A comparison between the optical spectra of an "empty" ARF and an MoS_2 integrated ARF, resulting in an average insertion loss due to the TMDC layers of around 7.5 dB in the 603 nm to 775 nm anti-resonant region. (b) The spectral results of the modulation process, showing decreased transmission for higher applied voltage. The insets show the mode images at the specified bias, with the near fundamental mode at low voltage transformed to a higher order mode at high voltage.

Funding. We acknowledge the support of the Engineering and Physical Sciences Research Council (EPSRC) funded National Hub in High Value Photonic Manufacturing through grant number EP/M015130/1 and the NSF Materials World Network EP/I035307/1.

Open Data The datasets of this work can be found at: https://doi.org/10.5258/SOTON/xxxx

Disclosures. The authors declare no conflicts of interest.

References

1. W. Belardi *et al.* Opt. Lett. **42**, 2535 (2017).
2. M. Nedeljkovic, R. Soref and G. Z. Mashanovich, IEEE Phot. Jour. **3**, 1171 (2011).
3. Z. Sun, A. Martinez and F. Wang, Nature Photonics **10,** 227 (2016).
4. H. Xia, *et al.* Opt. Express, **22**, 17341 (2014).
5. Y. Yu, *et al.* Nano Lett. **17,** 3613 (2017).
6. D. Vella, *et al.* 2D Materials **4,** 021005 (2017).
7. K-K. Liu, *et al.* Nano Lett. **12,** 1538 (2012).
8. J. Yang, *et al.* Nanoscale **7,** 9311 (2015).
9. H. Li, *et al.* Adv. Funct. Mat. **22,** 1385 (2012).
10. J. R. Sparks, *et al.* Jour. of Lightwave Tech. **29**, 2005 (2011).
11. W. Zhao, *et al.* Nanoscale **5,** 9677 (2013).
12. A. H. Lewis, *et al.* OSA Tech. Digest FW6B.4 (2018).
13. K.C. Kwon, *et al.* MRS comms. **7**, 272 (2017).
14. A.K.M. Newaz *et al.* Solid State Comms. **155**, 49 (2013).
15. F. Couny, *et al.* Science. **318,** 1118 (2007).
16. F. De Lucia, *et al.* Opt. Lett. **42**, 69 (2017).
17. B. Yan and C. Felser, Annu. Rev. Condens. Matter Phys. **8**, 337 (2017).

Full References

1. W. Belardi, F. De Lucia, F. Poletti, and P.J. Sazio, "Composite material hollow antiresonant fibers," Opt. Lett. **42**(13), 2535-2538 (2017).
2. M. Nedeljkovic, R. Soref, and G. Z. Mashanovich, "Free-Carrier Electrorefraction and Electroabsorption Modulation Predictions for Silicon Over the 1-14- µm Infrared Wavelength Range," IEEE Phot. Jour. **3**(6), 1171-1180 (2011).
3. Z. Sun, A. Martinez, and F. Wang, "Optical modulators with 2D layered materials," Nature Photonics **10,** 227-238 (2016).
4. H. Xia, H. Li, C. Lan, C. Li, X. Zhang, S. Zhang, and Y. Liu, "Ultrafast erbium-doped fiber laser mode-locked by a CVD-grown molybdenum disulfide (MoS2) saturable absorber," Opt. Express, **22**(14), 17341-17348 (2014).
5. Y. Yu, Y. Yu, L. Huang, H. Peng, L. Xiong, and L. Cao, "Giant Gating Tunability of Optical Refractive Index in Transition Metal Dichalcogenide Monolayers" Nano Lett. **17**(6), 3613-3618 (2017).
6. D. Vella, D. Ovchinnikov, D. Viola, D. Dumcenco, Y. C. Kung, E. A. A. Pogna, S. Dal Conte, V. Vega-Mayoral, T. Borzda, M. Prijatelj, D. Mihailovic, A. Kis, G. Cerullo, and C. Gadermaier "Field-induced charge separation dynamics in monolayer MoS_2," 2D Materials **4**(3), 021005 (2017).
7. K-K. Liu, W. Zhang, Y. H. Lee, Y. C. Lin, M. T. Chang, C. Y. Su, C. S. Chang, H. Li, Y. Shi, H. Zhang, C. S. Lai, and L. J. Li, "Growth of large-area and highly crystalline MoS2 thin layers on insulating substrates," Nano Lett. **12**(3), 1538-1544 (2012).
8. J. Yang, Y. Gu, E. Lee, H. Lee, S. H. Park, M-H. Cho, Y. H. Kim, Y-H. Kim, and H. Kim, "Wafer-scale synthesis of thickness-controllable MoS2 films via solution-processing using a dimethylformamide/n-butylamine/2-aminoethanol solvent system," Nanoscale **7,** 9311-9319 (2015).
9. H. Li, Q. Zhang, C. C. R. Yap, B. K. Tay, T. H. T. Edwin, A. Olivier and D. Baillargeat "From Bulk to Monolayer MoS_2: Evolution of Raman Scattering," Adv. Funct. Mat. **22**(7), 1385-1390 (2012).
10. J. R. Sparks, J. L. Esbenshade, R. He, N. Healy, T.D. Day, D. W. Keefer, P. J. Sazio, A. C. Peacock, and J. V. Badding, "Selective Semiconductor Filling of Microstructured Optical Fibers,", Jour. of Lightwave Tech. **29**(13) 2005-2008 (2011).
11. W. Zhao, Z. Ghorannevis, K. K. Amara, J. R. Pang, M. Toh, X. Zhang, C. Kloc, P. H. Tan, and G. Eda, "Lattice dynamics in mono- and few-layer sheets of WS_2 and WSe_2," Nanoscale **5**, 9677-9683 (2013).
12. A. H. Lewis, F. De Lucia, W. Belardi, C. C. Huang, J. R. Hayes, F. Poletti, D. Hewak, and P. J. Sazio, "Composite Material Hollow Core Optical Fiber Electro-Modulation" in Frontiers in Optics / Laser Science, OSA Technical Digest (Optical Society of America, 2018), paper FW6B.4.
13. K. C. Kwon, S. Choi, K. Hong, D. M. Andoshe, J. M. Suh, C. Kim, K. S. Choi, J. H. Oh, S. Y. Kim, and H. W. Jang, "Tungsten disulfide thin film/p-type Si heterojunction photocathode for efficient photochemical hydrogen production" MRS comms. **7**(2), 272-279 (2017).
14. A. K. M. Newaz, D. Prasai, J. J. Ziegler, D. Caudel, S. Roninson, R. F. Haglund Jr., and K. I. Bolotin, "Electrical control of optical properties of monolayer MoS_2," Solid State Comms. **155**, 49-52 (2013).
15. F. Couny, F. Benabid, P. J. Roberts, P. S. Light and M. G. Raymer, "Generation and Photonic Guidance of Multi-Octave Optical-Frequency Combs", Science 318, 1118 (2007).
16. F. De Lucia, D. W. Keefer, C. Corbari, and P. J. Sazio, "Thermal poling of silica optical fibers using liquid electrodes" Opt. Lett. **42**(1), 69-72 (2017)
17. B. Yan and C. Felser, "Topological Materials: Weyl Semimetals" Annu. Rev. Condens. Matter Phys. **8**, 337-354 (2017).